PII: S0955-2219(98)00073-9

Carbon Fiber-reinforced (YMAS) Glass-Ceramic Matrix Composites. II. Structural Changes in the Matrix with Temperature

W. Sinkler,[a]* M. Monthioux,[b] V. Bianchi,[c] P. Goursat[c] and E. Ménessier[d]

[a]Department of Materials Science and Engineering, Northwestern University, 8225 Sheridan Road, Evanston, IL 60208-3108, USA
[b]Centre d'Elaboration des Matériaux et d'Etudes Structurales, UPR A-8011 CNRS, B.P. 4347, F31055 Toulouse Cedex 4, France
[c]Laboratoire des Matériaux Céramiques et Traitements de Surface, Université de Limoges, UER Sciences, 123 Avenue Albert Thomas, F87060 Limoges Cedex, France
[d]Société Céramiques and Composites, BP 7, F65460 Bazet, France

Abstract

With the overall aim to study a specific family of carbon-reinforced glass-ceramic matrix composites, the structural and textural changes occurring within a glass belonging to the Mg–Al–Si–Y–O chemical system were investigated. Investigation techniques were mainly transmission electron microscopy, but also scanning electron microscopy, polarized light optical microscopy, X-ray diffraction, and thermal analysis. Some differences between the carbon (fiber)-containing material and the carbon-free material are revealed, mainly through local oxygen-depletions due to a reduction effect by carbon. Mainly, the way that the various phases allowed by the starting stoichiometry crystallize during an increasing heat-treatment is observed, i.e. magnesium aluminum silicate as indialite, yttrium silicate, magnesium aluminum oxide as spinel, in addition to corundum. Phases transformations, crystallized phase morphologies, and textural relationships between phases are among the features described.

Résumé

Dans le but plus général d'étudier une famille particulière de composites à matrice vitrocéramique à renfort carbone, les changements structuraux et structuraux intervenant au sein d'un verre appartenant au système chimique Mg–Al–Si–Y–O ont été examinés. Les différentes techniques d'investigation ont été essentiellement la microscopie électronique à

transmission, mais aussi la microscopie électronique à balayage, la microscopie optique en lumière polarisée, la diffraction des Rayons X, et l'analyse thermique. Quelques différences entre le verre contenant du carbone (sous forme de fibres) et le verre quand il n'en contient pas ont été révélées, qui se résument principalement à une sous-stoechiométrie locale en oxygène, due à un effet réducteur du carbone. L'essentiel du travail a consisté à observer les étapes de cristallisation des différentes phases permises par la stoechiométrie de départ, à savoir un silicate d'aluminium et de magnesium (indialite), un silicate d'yttrium, un oxyde d'aluminium et de magnésium (spinelle), en sus de corindon. Les morphologies de différentes phases, leur transformation, ainsi que leur relations texturales font partie des aspects étudiés. © 1999 Elsevier Science Limited. All rights reserved

1 Introduction

An extensive study of carbon-reinforced YMAS matrix composites has been performed from 1992 to 1995 in our laboratories,[1] and is now being published.[2–5] The main purpose was to investigate the relationships between the process conditions (fiber type, densification temperature and pressure), and the macroscopic mechanical properties of the composites.[1–3] As far as macroscopic features are due to microscopic causes, specifically in composites, changing the process conditions may have induced interfacial changes at the fiber/matrix

*To whom correspondence should be addressed.
E-mail: sinkler@apollo.numis.nwu.edu

contact, which were able to be related to changes in the mechanical behaviour.[2,4] On the other hand, the initial chemical composition of the matrix (within the Mg–Al–Si–Y–O system) was chosen not to be a parameter. Thus, because fibers were always carbon fibers, though from various origins,[3] the overall chemical composition of the matrix did not change from one composite to another. However, structural changes were observed in the matrix, which therefore may be claimed to be due to the effect of temperature only.

In addition, several papers have been devoted to the study of glasses, ceramics, and glass-ceramics materials from related chemical systems (Refs 6 and 7, for instance, and references therein). However, they have mainly dealt with the thermochemical description of the phase diagrams, i.e. few have been concerned with the microstructural characterization, or more specifically with imaging the textural aspects of the structural changes. Revealing how and when phases nucleate, grow, associate, and transform within a complex system under specific time/pressure/temperature conditions is believed to be as important as calculating the domains of phase occurrence through thermodynamics. Indeed, such calculations may not consider variations in energy due to some physical aspects (such as the effect of nanometric sizes for crystals, for instance),[8] and do not consider kinetics either. Thus, direct imaging of the crystallization mechanism of complex systems is useful to sustain the calculations and distinguish between various microstructural states.

This paper thus reports the structural and textural evolution of a SiO_2–MgO–Al_2O_3–Y_2O_3 glass in the 1000–1250°C range, mainly through transmission electron microscopy (TEM), but also using scanning electron microscopy (SEM), X-ray diffraction (XRD), and thermogravimetric analysis.

2 Experimental

2.1 Samples and preparation procedure for the composites

Composites were prepared at the Laboratoire des Matériaux Céramiques et Traitements de Surface (Limoges University). The preparation method has been extensively described in a previous paper.[3] Briefly, the main steps included a liquid impregnation route of the fiber tows (the slurry contained the glass powder, a solvent and some binding, wetting, etc., agents), a low temperature heat treatment (up to 425°C) in air to remove organic compounds without oxidizing the carbon fibers, then an oriented pressure sintering (graphite mold, the walls of which were coated with hexagonal BN

powder to prevent graphite/glass reactions) under argon (U Grade from Air Liquide). The heating and cooling rates were 25°C min⁻¹, with no pressure applied during these steps but the atmospheric pressure. The oriented pressure (10 MPa) was only exerted during 1 h (exceptionally 0·5 h) at 1050°C (exceptionally 1000, 1150, or 1200°C), i.e. at the end of the impregnation step. An annealing step at atmospheric pressure was then generally carried out, at various temperature/time conditions (Table 1).

Since the type of carbon fibers was a parameter for the overall study, results reported in this paper are concerned with composites reinforced with T400H (SOFICAR, France) PAN–based fiber or Thornel (AMOCO, USA) P25 or P55 pitch-based fibers. However, the influence of different fibre types on microstructural developement is expected to be negligible (all fibres being carbon), a point borne out by the results presented here.

The YMAS glass powder incorporated in the slurry was prepared by CERAMIQUES & COMPOSITES Company (Bazet, France) by melting all the oxide components but Al_2O_3 (1700°C under nitrogen in a carbon furnace), then quenching and grinding ($< 10 \mu m$). The molar composition is 36% SiO_2, 34·4% Al_2O_3, 20% Y_2O_3, 9·6% MgO, 0·3% Fe_2O. The YMAS glass powder itself thus prepared (dark gray colored) was also investigated as a bulk (i.e. not as a composite), though less extensively, in order to check whether it may behave differently while associated with carbon fibers or not. Various sintering conditions were used on the YMAS glass powder for this additional investigation, the conditions of which will be given in the text.

2.2 Investigation methods

The micro- and nanotextural and structural study was mainly performed with a transmission electron
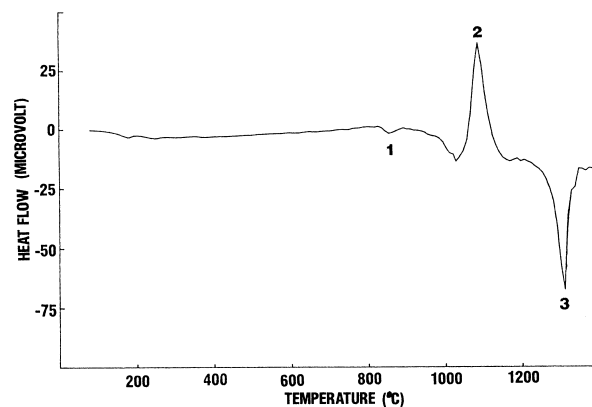

Fig. 1. YMAS glass powder. Differential thermal analysis obtained from a thermal treatment in an Al_2O_3 crucible from 20 to 1400°C with a 10°C min⁻¹ heating rate, oxygen atmosphere. Peak 1 corresponds to the glass transition, peak 2 corresponds to the main crystallisation, peak 3 corresponds to the melting of the bulk.

microscope (Philips CM12 TEM), using a 120 kV high voltage and a Super-twin objective lens. The microscope was also equipped with an energy dispersive X-ray analysis system (Edax), which was used to perform local and comparative chemical analysis on areas larger than 50 nm for elements with $Z > 5$. Other textural and chemical analyses were performed with a scanning electron microscope (JEOL 840 SEM) both through the detection of secondary electrons, back-scattered electrons and X photons from fluorescence. Textural and structural investigations at low magnification were performed using an optical microscope (Olympus BH2 OM) with polarized light (for areas larger than about 0·5 m, which is about the resolution power of the OM). Standard X RD investigations were also performed.

Some investigations were also performed using a thermogravimetry (TGA) and differential thermal analysis (DTA) system (Setaram TAG24, with symetrical configuration). When argon atmosphere was used, the furnace volume was previously purged using argon (N56 grade from Air Liquide) at least three times.

2.3 Preparation of samples prior to TEM investigation

Both the YMAS glass-ceramic and the composite materials were exclusively prepared using ion-milling. Small pieces of composites were trimmed then mechanically thinned using diamond tools then diamond and SiC powder suspensions and abrasive papers. The final step of mechanical thinning was performed on both sample faces using a dimple grinder (Gatan 656) with a diamond powder suspension (grain sizes were in the 2–4 μm range), in order to reach thicknesses close to about 30 μm. Ion-thinning was then performed (Gatan Duomill 600) using a 4 kV high voltage and final incidence angles of 12°.

Because the ceramic matrix is an insulator, it was usually necessary to deposit a thin (< 5 nm) carbon coating on the TEM foils by evaporation in order to avoid problems with charging in the TEM, likely to alter the quality of the micrographs.

3 Results

3.1 Evolution of the YMAS glass-ceramic (= as a bulk)

The changes in phases occurring within the YMAS glass powder with an increasing sintering temperature (2°C min^{-1}, 1·5 h dwell time, air atmosphere, normal pressure) was followed by XRD. This indicated the following broad temperature regimes which are summarized as follows:

- 850–950°C: the majority phase is amorphous, with minor amounts of pre-existing αAl_2O_3 (corundum) originating from the initial oxide constituent powder.

- 950–1100°C: rapid crystallization followed by very slow evolution (grain growth, phase changes) of $\alpha Mg_2Al_4Si_5O_{18}$ (high temperature hexagonal cordierite, = indialite) and $\alpha Y_2Si_2O_7$ (triclinic)[9] as main components, and $MgAl_2O_4$ (spinel) as a minor component.

- 1100–1200°C: transformation of $\alpha Y_2Si_2O_7$ to β–$Y_2Si_2O_7$ (high temperature monoclinic = keiviite).[9]

Some discrepancies may be found relative to the literature, regarding the α to β transformation temperature for $Y_2Si_2O_7$ for instance, reported to occur at 1225°C.[9] This may be due to kinetic effects and differences in the sintering conditions. Other examples will be given later.

In addition to XRD, DTA (oxygen atmosphere) was used to characterize phase changes occurring in the YMAS glass powder with increasing temperature. A DTA trace taken at 10°C min^{-1} is shown in Fig. 1. A glass transition is seen as a small endothermal peak (peak 1) between 815 and 855°C. Crystallization of the liquid is seen as a large exothermal peak (peak 2) extending from 945 to 1055°C. The point of fusion of the subsequent crystallized ceramic occurs at about 1300°C, as indicated by the last large endothermal peak (peak 3).

Density measurements of the YMAS glass showed a variation from 2·42 g cm^{-3} for the amorphous to 3·1 g cm^{-3} for the fully crystallized state.[8] Based on volume expansion measured in the 400–800°C temperature range, thermal expansion coefficients (CET) have been determined as $7·1 \times 10^{-6}$ and $6·3 \times 10^{-6}$ for the amorphous and crystalline states, respectively.[1,2]

A peculiar experimental detail revealed that the YMAS material was able to react chemically with carbon, which is of importance for its suitability in a carbon fiber-reinforced composite. Evidence for such a reaction was found in the specific optical absorption characteristics of the YMAS glass-ceramic (obtained from 1050°C pressureless sintering of the YMAS glass powder in a carbon furnace, nitrogen atmosphere). Like the starting powder, the material appeared black [Fig. 2(a)] and was opaque for thicknesses exceeding ≈ 200 μm.
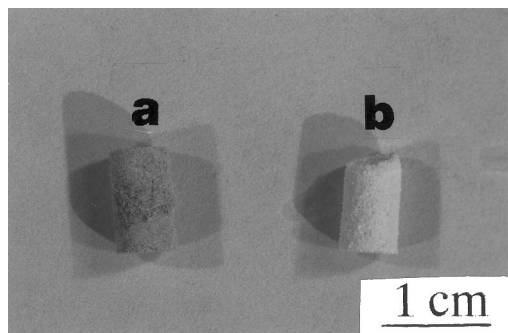
Fig. 2. Aspect of the 1050°C sintered (nitrogen atmosphere) YMAS glass-ceramic after a 1200°C annealing treatment (a) under argon, (b) under oxygen. The color changes from dark to clear indicating that the starting glass-ceramic material was under-stoichiometric with respect to the oxygen content.

As far as partial reduction of oxides can change optical absorption characteristics, it is thus likely that this unexpected color was due to such a partial reduction by the carbon of the furnace during the glass-ceramic preparation procedure. Support for a chemical reaction bertween YMAS and carbon was found from thermogravimetric investigation. The YMAS glass-ceramic was subsequently treated for 3 h at 1200°C either under oxygen or under argon (alumina furnace). This resulted in a change in color from black (YMAS glass-ceramic before and after 1200°C annealing under argon) to white (after 1200°C annealing under oxygen), as illustrated in Fig. 2(b), and a weight gain of 0·3% (compared to 0·1% weight gain under argon, presumably due to oxygen impurities in the gas). This indicates that the YMAS glass-ceramic material was under–stoichiometric with respect to oxygen.

Correspondingly, Fig. 3(a) shows the 1050°C-sintered (nitrogen atmosphere) YMAS glass–ceramic in OM using polarized light in transmission. The predominant color of the specimen is magenta, whichs indicates a predominantly amorphous state. Small inhomogeneities may be seen throughout the micrograph (often colored blue or yellow on the original slide) which indicates the presence of small crystals within an amorphous matrix. In addition, large opaque areas are present, which are not voids or bubbles [since not visible in reflected light, see Fig. 3(b)]. The strong light absorption in these regions suggests that conditions are locally achieved which have caused an enhancement of partial reduction. Figure 3(b) shows the same area using natural light in reflection. Small needle-like crystals which intersect the specimen surface are visible away from the large opaque areas (which are no longer revealed). A SEM image using backscattered electrons Fig. 4 indicates that the needle-like crystals contain light elements (they appear dark), and therefore are presumably Al_2O_3 (corundum), consistent
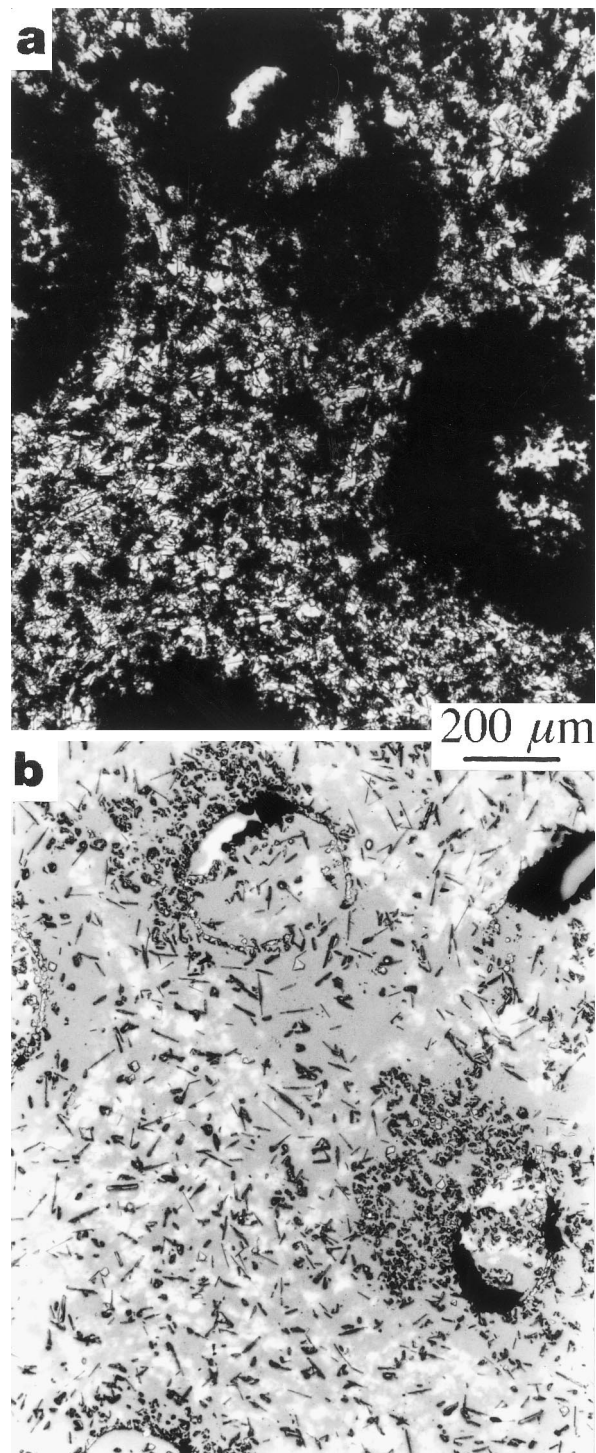

Fig. 3. 1050°C-sintered (nitrogen atmosphere) YMAS glass-ceramic. Black-and-white duplication of an OM image: (a) transmitted, polarised light. Black areas are assumed to be due to oxygen–depleted zones: (b) same region using reflected, natural light. The dark areas visible in (a) are associated with high concentrations of crystals, which are probably indialite. Needle-like crystals are probably corundum.

with the EDX measurements subsequently performed on the matrix of the composite. The large opaque areas [they can be located using Fig. 3(a)] contain high concentrations of smaller, isometric polyhedral crystals, which suggests that enhanced partial reduction is related to the phase
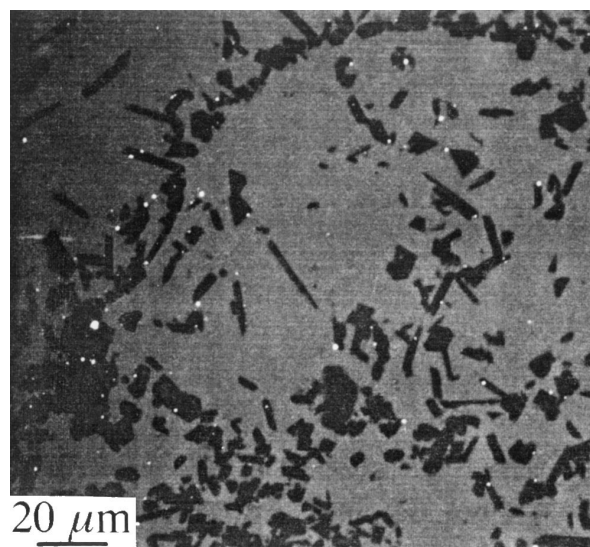
Fig. 4. 1050°C-sintered (nitrogen atmosphere) YMAS glass-ceramic. SEM image (back-scattered electrons). Dark crystals are either corundum or indialite, i.e. yttrium-free phases. Correspondingly, the bulk appears gray, due to its yttrium content.

Fig. 5. 1000°C-sintered (air atmosphere) YMAS glass-ceramic. SEM image (back-scattered electrons): (a) low magnification; (b) higher magnification of the aggregate arrowed in (a). Dark feather-like crystals are cordierite, white parts between them are yttrium silicate; (c) higher magnification of the bulk surrounding the aggregates. Arrow indicates an example of a star-like morphology typical of a primary crystallisation for cordierite crystals. Cordierite crystals(dark parts) are again found associated with yttrium silicate or at least yttrium-rich areas (clear parts).

crystallization. From the SEM image in Fig. 4, these crystals again contain light elements, which suggests that polyhedral crystals are cordierite ($Mg_2Al_4Si5O_{18}$), and that crystallization of the latter may be enhanced by oxygen depletion or, more probably, may have induced it. A possible mechanism is that the crystallization of cordierite has locally enhanced the reduction effect (initiated by the carbon of the furnace during the glass preparation procedure) by taking out from the matrix the amount of oxygen atoms required to reach the appropriate stoichiometry. No such effect was associated with corundum crystals since the latter did not melt and directly originate from the starting oxide powder.

In Fig. 4, beside the light elements-containing cordierite and corundum crystals which appear dark, the bulk part of the glass appears grey (i.e. with a lighter contrast), due to the contribution of yttrium ($Z = 39$) which did not crystallized yet as a silicate, or has actually crystallized but with grain sizes below the resolution power.

Opaque areas due to oxygen depletion are no longer observed in YMAS ceramics resulting from the sintering in air of the YMAS powder. The microstructure after such sintering at 1000 and 1200°C is illustrated with backscattered electrons images from SEM in Figs 5 and 6 respectively. Figure 5(a) shows how cordierite (dark crystals) may nucleate either as spheroidal aggregates [arrow in Fig. 5(a)] in which it is associated with yttrium silicate [bright areas interspersed with dendritic cordierite crystals in Fig. 5(b)], or as smaller star-like associations disseminated in the bulk
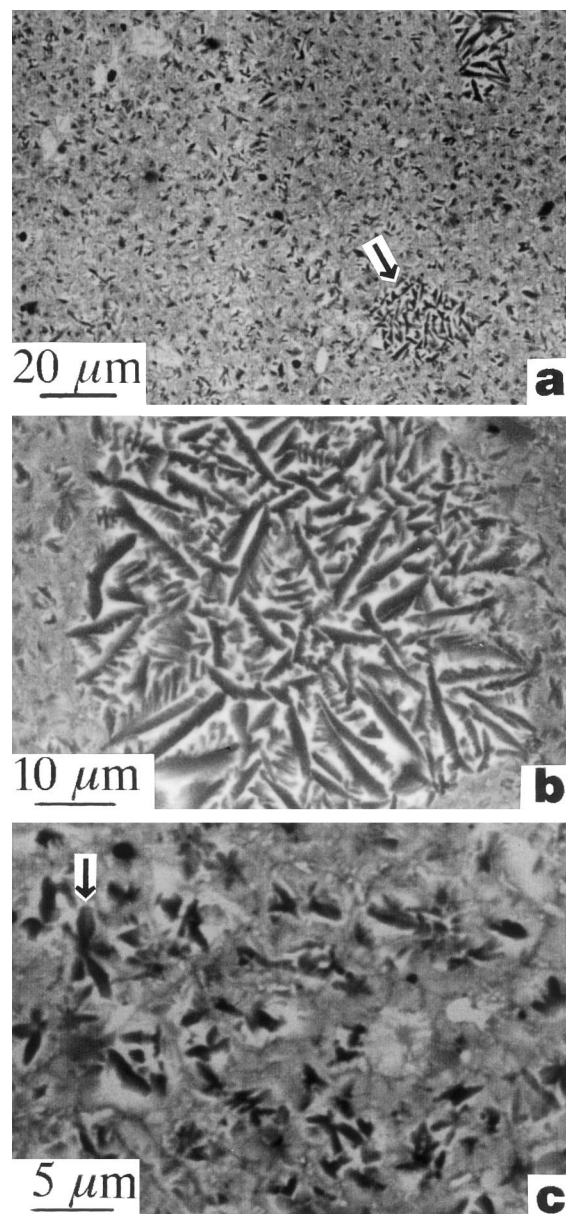
[arrow in Fig. 5(c)]. It is noteworthy that cordierite seems to be associated with yttrium-rich areas again, though at a primary step of the crystallization. Indeed, dark parts (cordierite) are most often surrounded by clearer parts (yttrium-bearing material) in Fig. 5(c). As soon as the temperature is sufficient for coarsening of the microstructure [1200°C, Fig. 6(a)–(b)], the peculiar association coalescence between the cordierite and yttrium silicate is lost.

It should be noted that no direct comparison is possible of the results of Figs 5 and 6 (YMAS

powder after 1000 and 1200°C sintering under air) with Figs 3 and 4 (YMAS powder after 1050°C sintering under nitrogen) concerning the crystallization progress, due to differences in the heat-treatment conditions, in particular holding time and atmosphere.

3.2 Evolution of the YMAS matrix (= within carbon fiber-reinforced composites)

As described in detail below, four main steps in the microstructure evolution of the YMAS material as a matrix in a carbon-reinforced composite may be distinguished using XRD (Fig. 7) and TEM. The various steps in the microstructural development with increasing temperature/time conditions are summarized according to the following scheme:

- Step 1: Majority phase is amorphous, with pre-existing αAl_2O_3 (corundum) and subsidiary amounts of $MgAl_2O_4$ (spinel) and $A Mg_2Al_4Si_5O_{18}$ (indialite) cordierite. This corresponds to sintering temperatures $\leq 1000°C$.

- Step 2: Rapid crystallization of indialite and $\alpha Y_2Si_2O_7$ as major components, which are associated in an eutectic-type microstructure. $MgAl_2O_4$ is present as a minor component. Subsidiary $\beta Y_2Si_2O_7$ (keiviite) is also already present. This corresponds to a narrow temperature range, around 1000–1050°C. Up to $\approx 1200°C$, it is followed by the domain of structural stability (no change in the X-RD spectra).

- Step 3: Coarsening of lamellar eutectic-type microstructure, evident by distortions of lamellae. Rapid transformation of $\alpha Y_2Si_2O_7$ to $\beta Y_2Si_2O_7$.

- Step 4: Overall α to β transformation of $Y_2Si_2O_7$, though the α structure is still present. Dramatic coarsening of all phases. Corundum or spinel with submicron grain sizes are no longer found. Loss of lamellar cordierite/yttrium silicate microstructure and development of globular microstructure. This may correspond to a 1200–1250°C range.

The heat treatments of the composites in the study are given, along with their degree of microstructural development from the above classification scheme, in Table 1. The classification is valid for holding time of approximately 1 h at the temperatures mentioned. While the temperatures characteristic
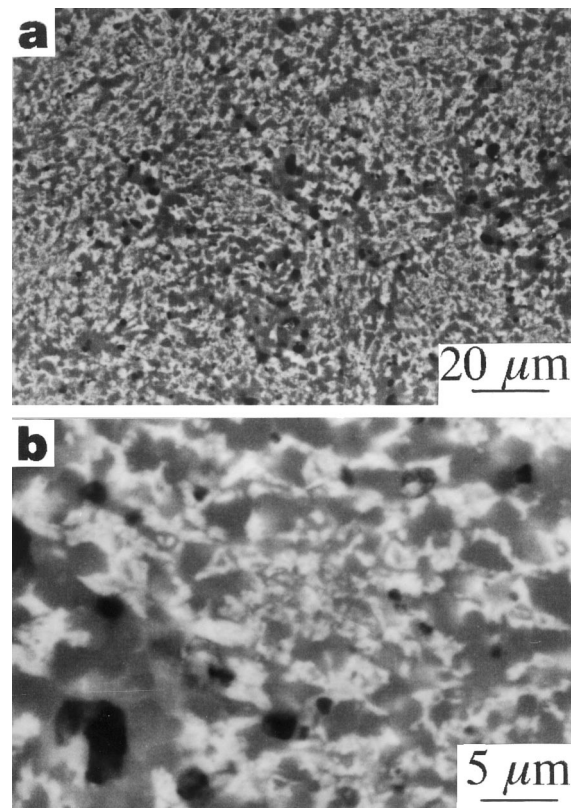

Fig. 6. 1200°C-sintered (air atmosphere) YMAS glass-ceramic. SEM image (back-scattered electrons): (a) low magnification; (b) higher magnification. Peculiar textures revealed in Fig. 5 have disappeared, due to the widespread growth and subsequent coalescence of crystallized areas.
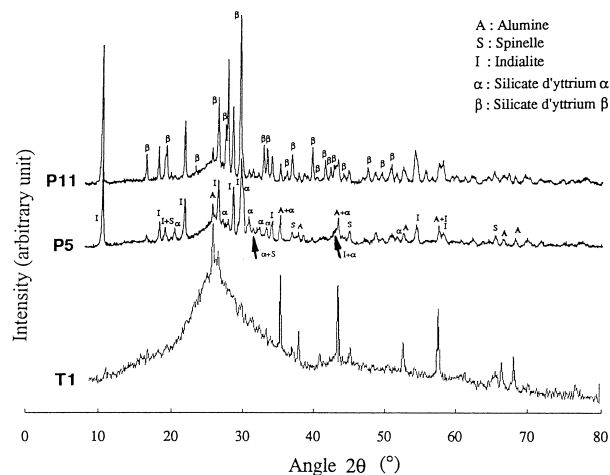

Fig. 7. YMAS matrix in composites. XRD spectra. Heat-treatment temperature increases from bottom to top. Sample code numbers refer to Table 1. T1, P5 and P11 correspond to Step 1, 2 and 4, respectively (see text). Peaks labelling is as follows: A = corundum, S = spinel, I = indialite, $\alpha = \alpha$-$Y_2Si_2O_7$, $\beta = \beta$-$Y_2Si_2O_7$.

of a particular step in microstructure development are generally consistent with the classification in Table 1, one of the composites (P7) was heat-treated (annealed) for a significantly longer time. This causes the microstructure development to correspond to a further advanced state than its heat

Table 1. Correspondence between the sample references, the conditions they were submitted to, and the various steps as they are defined in the text for the YMAS matrix evolution.

Reference		Sintering conditions (with pressure)	Annealing conditions (without pressure)	Crystallization step
Paper	Laboratory			
T1	C4-2	1000°C/1h	—	1
P3	C3-5	1000°C/1h	—	1
P5	C5-3	1050°C/1h	—	2
P13	C7-1	1050°C/1h	—	2
P6	C5-5	1050°C/1h	1050°C/1·5h	2
P14	C7-2	1100°C/1h	—	2
T5	C4-4	1150°C/1h	—	2
T6	C8-1	1200°C/1h	—	2
P7	C6-2	1050°C/1/h	1050°C/6h	3
P10	C10-2	1050°C/0.5h	1250°C/0·5h	4
P11	C6-3	1050°C/1h	1250°C/1·5h	4
T7	C8-2	1050°C/1h	1250°C/1·5h	4

The first column refers to the sample references as they are used in the companion articles about the work.[1,3–5] The second column is for internal use only.

treatment temperature would suggest (e.g. more advanced than for the 1200°C-sintered composite T6). This again indicates that kinetics is very important, specifically in the temperature range where the crystallization occurs. Actually, the overall α to β transformation temperature for $Y_2Si_2O_7$ is now more consistent with literature[9] using the sintering and heat treatment conditions of Table 1 than it was for the YMAS bulk glass (see Section 3.1 above). However, based on the above scheme, the development of the YMAS material as a matrix in a composite does not differ substantially from that observed for the YMAS material as a bulk glass, despite some evidence of the glass reduction by carbon. The probable reason is that the starting glass powder was the same for both materials, and had already been submitted to a carboreduction effect during the glass powder preparation procedure (due to the use of a carbon furnace). Discrepancies (e.g. the crystallization state at 1000°C is more advanced for the composite than for the bulk) are believed to be rather due to the differences in the thermal treatment conditions, such as the absence (bulk YMAS glass) or the presence (YMAS matrix composites) of oriented pressure during sintering (likely to inhibit structural rearrangements).

Figure 8 shows a low magnification OM image (polarized light, in transmission) of the composite P3 with a microstructure corresponding to Step 1. Due to their strong absorbance, carbon fibers appear as dark circles in the micrograph, surrounded by the MAS-Y matrix, the overall color of which was magenta (light gray in the figure) indicating a main amorphous state. Some large ($\approx 5\,\mu m$) crystals were detected as blue (single arrow) or yellow (double arrows) regions in the

micrograph. These are likely of corundum, due to the small size of all other crystalline phases at this stage, as revealed by TEM below. Also, it can be noticed than the matrix tends to be darker close to the carbon fibers than away from them, consistent with the reduction effect by carbon revealed in the study of the YMAS glass (Section 3.1).

Figure 9 presents a SEM image (back scattered electrons) of a similar area in composite P3. The carbon fibers appear dark due to their low back-scattering yield. Crystals in the matrix are visible as dark areas also, indicating yttrium-free phases (corundum, and early crystallized cordierite and spinel). The yttrium-containing glassy phase appears an intermediate gray (yttrium is the only heavy element in the composite). X-EDS confirmed that crystals with elongated morphologies tend to
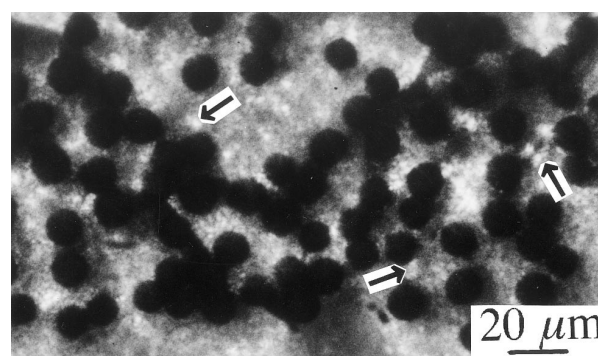

Fig. 8. YMAS matrix in composite P3, at Step 1 (see text). Black-and-white duplication of an OM color image (transmitted, polarized light). Round parts are carbon fibers, which appear dark because of the high absorbance of polyaromatic carbon for visible light. The gray contrast of the matrix corresponds to magenta, indicating amorphous state. However, single or double arrows indicate blue or yellow areas (light gray contrast) which reveal the occurrence of crystallized phases (corundum).

be corundum (double arrow). Cordierite crystals with more equiaxed morphologies could occasionally also be resolved (single arrow). A few exceptional crystals of yttrium silicate were also detected, appearing as the bright areas in Fig. 9; their compositions were checked using X-EDS. They are present in very small quantity, and were thus not resolvable using XRD. The microscopic appearance of cordierite precipitates at Step 1 is illustrated using TEM in Fig. 10. The radial leaf-like form is consistent with the SEM image shown as Fig. 5(c), although the size is significantly smaller, indicating that a more advanced stage in the microstructure development was reached in Fig. 5(c). In Fig. 10 are also imaged small spinel crystals (single arrow) exhibiting a specific spherical morphology, and a corundum crystal (large crystal, double arrow).

Step 2 is illustrated in Figs 11–13. In OM, using transmitted, polarised light, an obvious color change from magenta to orange-pink was observed with respect to the Step 1 matrix. This is consistent with a fine-crystalline matrix, in which optically anisotropic domains, in addition to some remaining amorphous phase (isotropic = magenta), are superimposed in the specimen cross-section. In a SEM image shown in Fig. 11 (back-scattered electrons), large crystals of yttrium silicate are now evident, and appear white in the micrograph. They
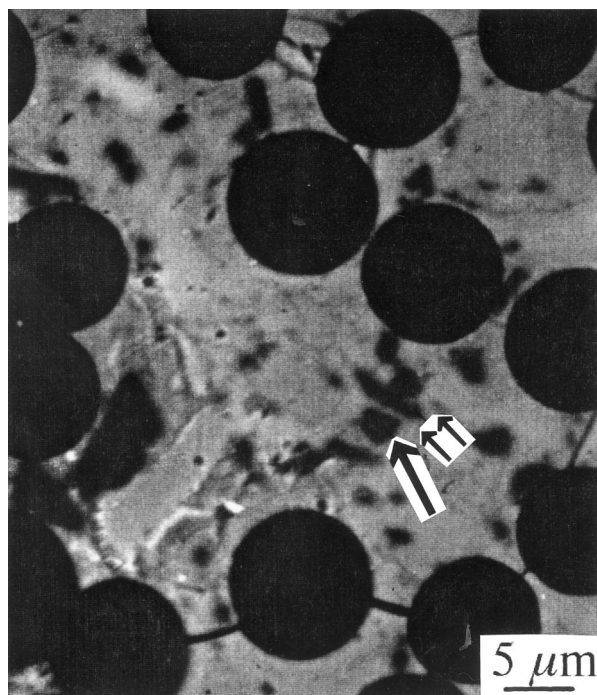
exhibit a star-like structure similar to that seen for cordierite, but at a larger scale. Dark crystals, corresponding to corundum and cordierite (spinel crystals are unlikely, since too small), are also visi-
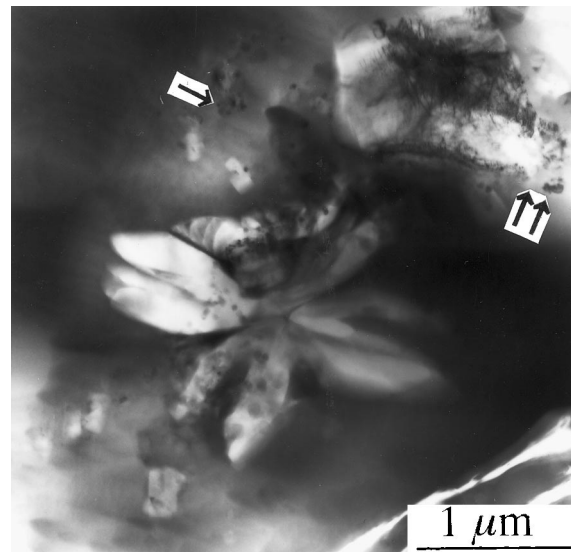

Fig. 10. YMAS matrix in composite T1, at Step 1 (see text). Low magnification TEM image. Peculiar star-like morphology for cordierite at a primary crystallization step, to be compared to similar textures revealed in the MAS-Y glass by SEM [Fig. 5(c)]. Single arrow indicates a spinel crystal with a characteristic spherical morphology, double arrow indicates a corundum crystal.
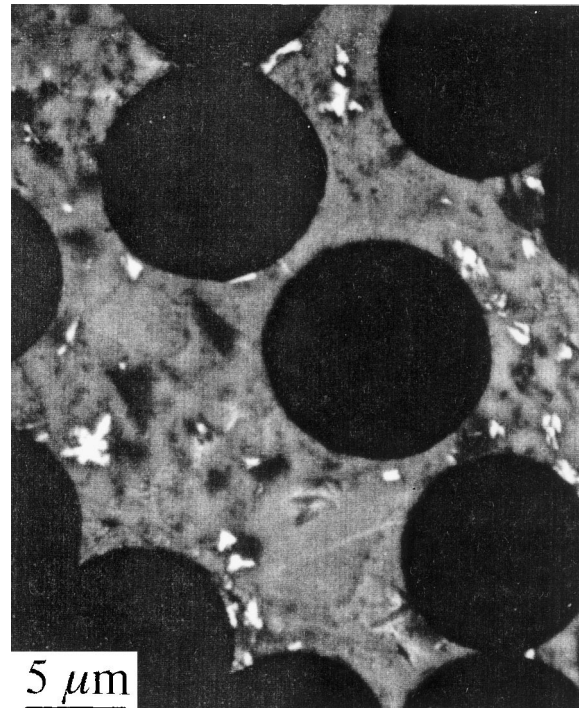

Fig. 9. YMAS matrix in composite P3, at Step 1 (see text). SEM image (back-scattered electrons). Round parts are carbon fibers, which appear dark because of their very low Z number. Other dark parts are yttrium-free crystals (single arrow = cordierite, double arrow = corundum, as determined from X-EDS). Clear parts contain Y–Si–O. Straight dark lines joining fibers are cracks.

Fig. 11. YMAS matrix in composite P5, at Step 2 (see text). SEM image (back-scattered electrons). Round parts are carbon fibers, which appear dark because of their low Z number. Other dark (polyhedral) parts are cordierite or corundum. Bright parts are yttrium-rich crystals (probably silicate) exhibiting the star-like morphology specific of a primary crystallisation state, as already observed for cordierite [Figs 5(c) and 10]. The gray contrast of the bulk indicates that most of the yttrium is still disseminated in the matrix.

ble in the matrix. The remainder of the matrix is now an intermediate gray, indicating that some yttrium remains here (by comparison to the crystals containing only lighter element than Si, which are darker). The microstructure in these intermediate gray regions could not be resolved using SEM. At higher magnification, in TEM, a peculiar crystalline microstructure was resolved in such region, which consisted of alternating bands less than 100 nm in width of cordierite and yttrium silicate, as shown in Fig. 12. In the micrograph, the yttrium silicate appears dark due to yttrium's stronger inelastic scattering. Additional crystals present in Fig. 12 are corundum (single arrow) and spinel (double arrow).

Figures 11 and 12 indicate the existence of two populations of yttrium silicate at this stage: one population is star-shaped and has large morphology on the order of $1\,\mu m$ resolvable by SEM (Fig. 11). The other has lamellar alternating band microstructure (Fig. 12). Lamellar microstructures such as this are typical of eutectic decomposition transformations, which suggest the presence of such an eutectic in the cordierite/yttrium silicate system. XRD (Fig. 7) has revealed that both $\alpha Y_2 Si_2 O_7$ and $\beta Y_2 Si_2 O_7$ (keiviite) are present in the material at this stage. While it was possible to verify using electron diffraction that the yttrium silicate of the lamellar eutectic microstructure was the α form at this stage, none of the star-like yttrium silicate population was observed in TEM due to its sparse and irregular distribution in the composite

and the small observable areas in TEM specimen. The phase of the second yttrium silicate population could therefore not be verified.

Electron diffraction of the eutectic bands of cordierite and $\alpha Y_2 Si_2 O_7$ had a single-crystalline aspect, indicative of a structural relationship between the two phases. Based on high resolution micrographs such as Fig. 13, it could be determined that the (002) planes of orthorhombic cordierite are parallel to the interfaces of the lamellae. Using electron diffraction and analysis of high resolution TEM micrographs, a provisional orientation relationship between $\alpha Y_2 Si 2O_7$ and cordierite was determined, such that: $(\bar{1}01)_\alpha$ $//(001)_c$ and $(001)_\alpha$ $//(021)_c$ where the subscripts α and c are for yttrium silicate and cordierite, respectively. In addition to the latter crystalline phases, large crystals of corundum (Fig. 12, single arrow), possibly already present prior to composite production, and round-shape spinel crystals exhibiting a specific
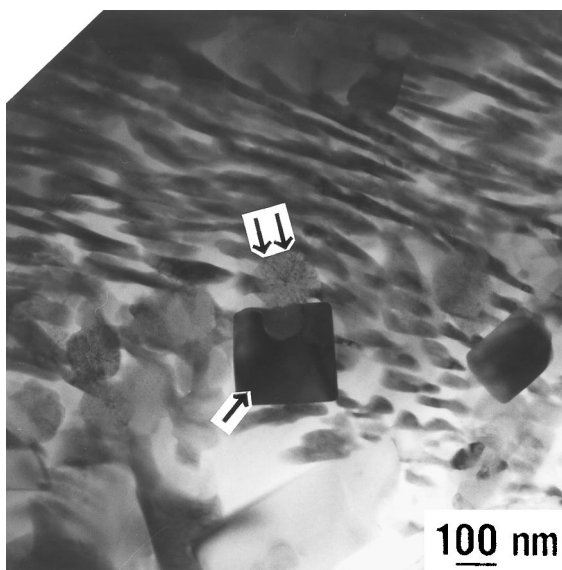

Fig. 12. YMAS matrix in composite P5, at Step 2 (see text). Low magnification TEM image. Alternate dark and clear bands are $\alpha Y_2 Si_2 O_7$ and $\alpha Mg_2 Al_4 Si_5 O_{18}$ (indialite), respectively, which is a typical eutectic microstructure. Single arrow indicates a corundum crystal. Double arrows indicate spinel crystals. The dark contrast of the yttrium silicate bands is due to the high Z number of yttrium. The dark contrast of the corundum crystals is due to excess thickness.
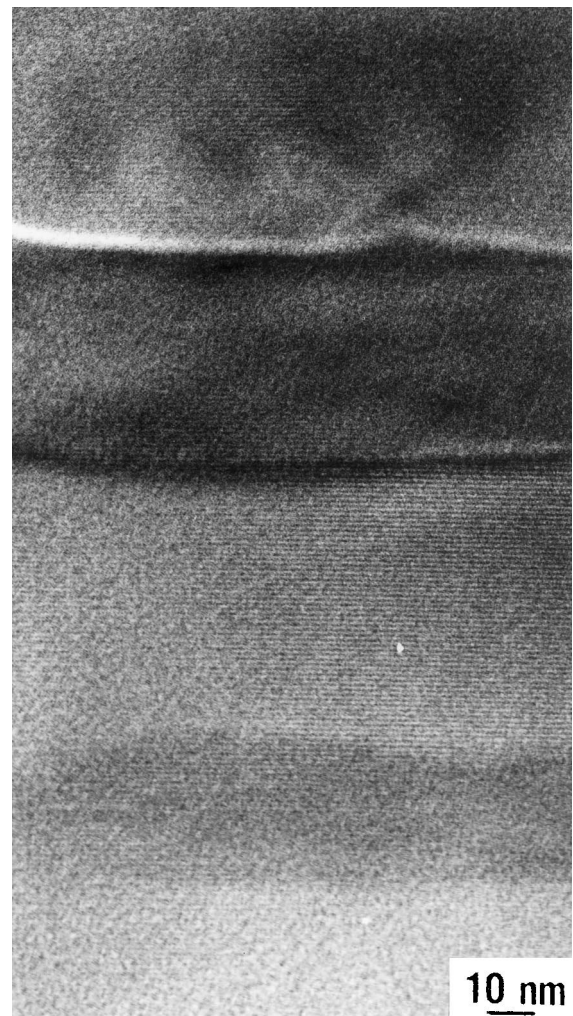

Fig. 13. YMAS matrix in composite P13, at Step 2 (see text). The lattice period is that of (002) planes from indialite at 0·467 nm. Though separated by $\alpha Y_2 Si_2 O_7$ bands, the indialite bands exhibit the same cristallographic orientation. The $\alpha Y_2 Si_2 O_7$ lattice was not under the Bragg angle and therefore was not imaged.

spherulitic aspect (Fig. 12, double arrow) were also found.

The composite representative of Step 3 (P7) was annealed for an extended time of 6 h at 1050°C (see Table 1). The XRD spectrum did not differ at this point from that after Step 2, and no significant differences were detected in SEM. Figure 14 shows a TEM image of the lamellar cordierite/yttrium silicate microstructure corresponding to that discussed above for Step 2. The wavy form of the lamellae is indicative of the beginning of a morphology change for the lamellar microstructure, due to the beginning of coarsening, and possibly driven by a minimization of the surface area associated with the microstructure. In addition, the $Y_2Si_2O_7$ crystals exhibit numerous stacking faults at this stage (Fig. 15) which are not observed at Step 2. This is presumably related to the gradual $\alpha \rightarrow \beta$ transformation of $Y_2Si_2O_7$. The fundamental planes parallel to the stacking disorder evident in Fig. 16 are consistent with the $(0\bar{1}1)$ planes

of the $\alpha Y_2Si_2O_7$ structure reported by Liddell and Thompson.[9] It is likely that the change in morphology and the structural $\alpha \rightarrow \beta$ transformation are related as the developement of $\beta Y_2Si_2O_7$ would change the cordierite/yttrium silicate interface structure. This may result in a loss of coherency and an increase in the surface energy, which would increase the driving force for morphological change and/or coarsening.

The final step in the microstructure evolution of the YMAS matrix, Step 4, is represented by

Fig. 15. YMAS matrix in composite P7, at Step 3 (see text). High resolution TEM image. The $\alpha Y_2Si_2O_7$ lattice now exhibits a peculiar contrast revealing stacking faults. This might precede the $\alpha \rightarrow \beta$ transformation.

Fig. 14. YMAS matrix in composite P7, at Step 3 (see text). Low magnification TEM image. The lamellar eutectic microstructure deforms, and lamellar crystals tend to become spherical.
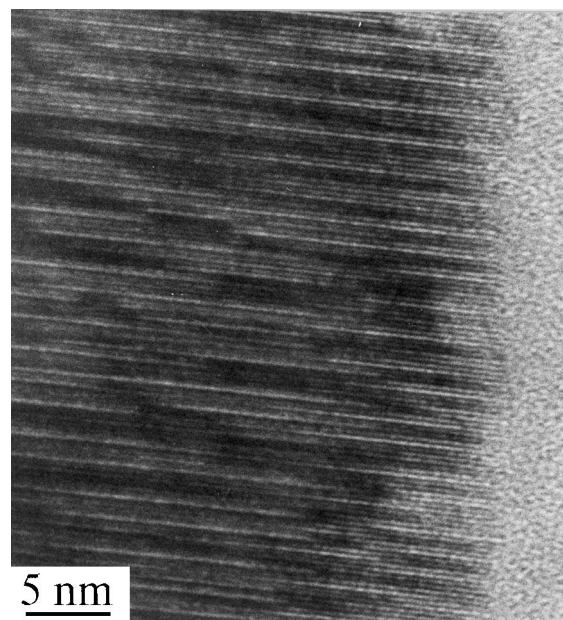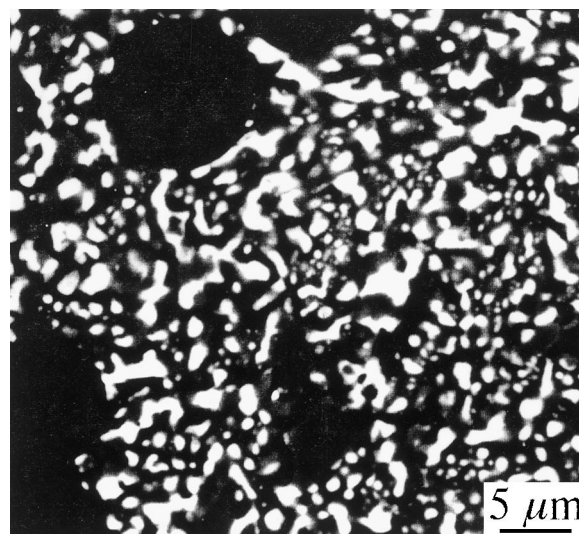

Fig. 16. YMAS matrix in composite P11, at Step 4 (see text). SEM image (back-scattered electrons). Both carbon fibers and the remaining bulk have now a similar dark contrast, due to the widespread concentration of yttrium into large keiviite crystals. Most of the keiviite crystals now exhibit a round morphology, the sizes of which are large enough to be imaged by SEM. Elongated crystals are inherited from the previous lamellar microstructure.

composites annealed at 1250°C (Table 1). In this step, a dramatic coarsening of the crystalline phases occurs, which is illustrated in Figs 16 and 17. Elongated or roughly spherical crystals of $Y_2Si_2O_7$ with sizes up to several micrometers are seen in SEM images (Fig. 16). These are not seen in the previous steps, and indicate a substantial decomposition of the lamellar yttrium silicate/cordierite microstructure. The TEM image shown in Fig. 17 indicates that smaller ($\approx$ 100 nm) globular yttrium silicate crystals also still exist, which appear as islands in a cordierite matrix. Based on XRD, most of the yttrium silicate is in the β phase (keiviite) at this point. Interestingly, small corundum or spinel crystals such as are present in Step 2 (Fig. 12) are no longer found in TEM, indicating a dramatic coarsening of these two phases.

Further heat-treatment would have induced the melting of the matrix, around 1300°C (Fig. 1).
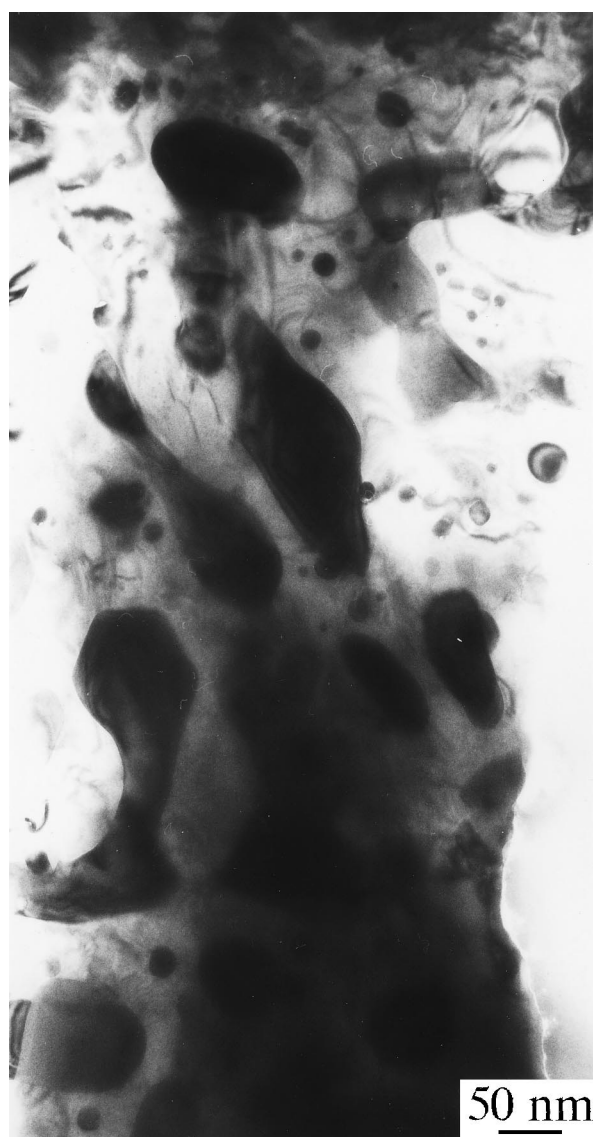

Fig. 17. YMAS matrix in composite T7, at Step 4 (see text). Low magnification TEM image. Yttrium silicate crystals (dark areas) are no longer as lamellae but more and more as single spherical crystals.

4 Conclusion

The changes occurring within a YMAS glass-ceramic have been studied with respect to both phase content and microstructure (morphology, size, spatial relationships between phases, crystallographic structure) as the matrix of carbon-reinforced composites. The primary crystallization of the high temperature form of cordierite (indialite) and spinel occurs first, with a very rapid kinetics, followed by that of $\alpha Y_2Si_2O_7$, which coexist with pre-existing corundum crystals. Following this is the formation of an eutectic-type microstructure of cordierite and yttrium silicate, in which these phases are associated in a crystallographic orientation relationship in alternating lamellae. Accompanying the precipitation of the lamellar microstructure is a fine precipitation of additional (secondary) corundum. Though the overall $\alpha \rightarrow \beta$ $Y_2Si_2O_7$ transformation occurs afterwards, it starts early with slow kinetics, ensuring that both structures (α and β) are always found together whatever the temperature, but with proportions consistent with the respective occurrence domains expected from literature. In a final stage, the overall α to β transformation of $Y_2Si_2O_7$ is associated with an overall coarsening and the gradual disappearance of the lamellar microstructure, which may indicate the loss of a low-energy coherent α-$Y_2Si_2O_7$/cordierite interface in the transformation to β-$Y_2Si_2O_7$.

Though some evidence of a reduction effect of the glass by carbon was found, the YMAS glass behaves similarly, regardless of whether it is heat-treated as a bulk or associated with carbon fibers.

References

1. Bianchi, V., Composites à fibres de carbone et matrice YMAS: elaboration, microstructure, comportements mécanique et tribologique. Ph.D. thesis 1995–22, Université de Limoges, France, 1995.
2. Bianchi, V., Goursat, P., Ménessier, E., Sinkler, W. and Monthioux, M., C/YMAS composites—effects of the interface and the residual stresses on the rupture behaviour. In Proceedings of the 8th CIMTEC, World Ceramic Congress, June 29–July 4, Florence, Italy. *Advanced Structural Fiber Composites. Adv. Sci. Technol.*, 1994, **7**, 695–702.

3. Bianchi, V., Goursat, P., Sinkler, W., Monthioux, M. and Ménessier, E., Carbon fiber reinforced YMAS composites. I. Preparation, structure and fracture strength. *Journal of the European Ceramic Society*, 1997, **17**, 1485–1500.
4. Bianchi, V., Goursat, P., Sinkler, W., Monthioux, M. and Ménessier, E., Carbon fiber reinforced YMAS composites. III. Interfacial aspects. *Journal of the European Ceramic Society*, in press.
5. Bianchi, V., Platon, F., Goursat, P. and Ménessier, E., Carbon fiber reinforced YMAS composites. IV. tribological behaviour, in press.
6. Derré, A., Ducarroir, M. and Allibert, M., System Si–Al–Mg–O: thermodynamic aspects of its influence on the oxidation resistance of silicon carbide at high temperature. *Journal of the European Ceramic Society*, 1994, **14**, 53–59.
7. Hampshire, S., Nestor, E., Flynn, R., Besson, J.-L., Rouxel, T., Lemercier, H., Goursat, P., Sebai, M., Thompson, D. P. and Liddell, K., Yttrium oxynitride glasses: properties and potential for crystallisation to glass-ceramics. *Journal of the European Ceramic Society*, 1994, **14**, 261–273.
8. Bigarre, J., Etude de la cristallisation et de propriétés mécaniques de vitrocéramiques du type YMAS. DEA Report, Université de Limoges, 1991, France.
9. Liddel, K. and Thompson, D. P., X-ray diffraction data for yttrium silicates. *Br. Ceram. Trans. J.*, 1986, **85**, 17–22.